

An SOT-switchable micromagnet scheme of adiabatic geometric gates for silicon spin qubits

Fang-Ge Li(李方阁), Ranran Cai(蔡冉冉), Bao-Chuan Wang(王保传), Hai-Ou Li(李海欧), Gang Cao(曹刚), and Guo-Ping Guo(郭国平)

Citation: Chin. Phys. B, 2025, 34 (**11**): 110306. DOI: 10.1088/1674-1056/addcd3
http://cpb.iphy.ac.cn; http://iopscience.iop.org/cpb

What follows is a list of articles you may be interested in

Robust quantum gate optimization with first-order derivatives of ion-phonon and ion-ion couplings in trapped ions

Jing-Bo Wang(汪景波)
Chin. Phys. B, 2025, 34 (**4**): 040302. DOI: 10.1088/1674-1056/adb40e

Correcting on-chip distortion of control pulses with silicon spin qubits

Ming Ni(倪铭), Rong-Long Ma(马荣龙), Zhen-Zhen Kong(孔真真), Ning Chu(楚凝), Wei-Zhu Liao(廖伟筑), Sheng-Kai Zhu(祝圣凯), Chu Wang(王儲), Gang Luo(罗刚), Di Liu(刘頓), Gang Cao(曹刚), Gui-Lei Wang(王桂磊), Hai-Ou Li(李海欧), and Guo-Ping Guo(郭国平)
Chin. Phys. B, 2025, 34 (**1**): 010308. DOI: 10.1088/1674-1056/ad8db1

Simulations of superconducting quantum gates by digital flux tuner for qubits

Xiao Geng(耿霄), Kaiyong He(何楷泳), Jianshe Liu(刘建设), and Wei Chen(陈炜)
Chin. Phys. B, 2024, 33 (**7**): 070305. DOI: 10.1088/1674-1056/ad47ab

A quantum blind signature scheme based on dense coding for non-entangled states

Ke Xing(邢柯), Ai-Han Yin(殷爱菡), and Yong-Qi Xue(薛勇奇)
Chin. Phys. B, 2024, 33 (**6**): 060309. DOI: 10.1088/1674-1056/ad2bed

Remote entangling gate between a quantum dot spin and a transmon qubit mediated by microwave photons

Xing-Yu Zhu(朱行宇), Le-Tian Zhu(朱乐天), Tao Tu(涂涛), and Chuan-Feng Li(李传锋)
Chin. Phys. B, 2024, 33 (**2**): 020315. DOI: 10.1088/1674-1056/ad1747

An SOT-switchable micromagnet scheme of adiabatic geometric gates for silicon spin qubits

Fang-Ge Li(李方阁)[1,2], Ranran Cai(蔡冉冉)[1,2,†], Bao-Chuan Wang(王保传)[1,2], Hai-Ou Li(李海欧)[1,2,3], Gang Cao(曹刚)[1,2,3,‡], and Guo-Ping Guo(郭国平)[1,2,3,4]

[1] *Chinese Academy of Sciences (CAS) Key Laboratory of Quantum Information, University of Science and Technology of China, Hefei* 230026, *China*
[2] *CAS Center for Excellence in Quantum Information and Quantum Physics, University of Science and Technology of China, Hefei* 230026, *China*
[3] *Hefei National Laboratory, University of Science and Technology of China, Hefei* 230088, *China*
[4] *Origin Quantum Computing Company Limited, Hefei* 230088, *China*

(Received 9 April 2025; revised manuscript received 23 May 2025; accepted manuscript online 26 May 2025)

Geometric phase gates have attracted considerable attention due to their intrinsic robustness against certain types of noise. Significant progress has been achieved in implementing geometric phase gates using microwave control in silicon-based electron spin systems. In this work, we propose an alternative geometric phase gate protocol that differs fundamentally from microwave driving approaches by leveraging square-wave control of rapidly switchable micromagnets driven by spin–orbit torque (SOT) to achieve fast and precise magnetic field modulation. By employing square-wave currents to control magnetization switching, our approach relaxes the requirements on waveform precision while significantly suppressing crosstalk. Moreover, our scheme inherently preserves trajectory closure at the end of each operation, effectively mitigating noise-induced path deviation and enhancing gate robustness even under strong noise conditions, thereby offering a promising pathway toward efficient and reliable quantum operations in large-scale qubit arrays.

Keywords: silicon spin qubit, geometric phase gate, spin–orbit torque, gate operation

PACS: 03.67.Lx, 85.35.Be, 85.75.–d, 73.61.Cw

DOI: 10.1088/1674-1056/addcd3 **CSTR:** 32038.14.CPB.addcd3

1. Introduction

Silicon-based spin qubits,[1] known for their exceptional coherence properties[2,3] and scalability,[4] have emerged as one of the most promising platforms for fault-tolerant quantum computing. Significant breakthroughs have been achieved in high-fidelity single-qubit operations,[3,5] two-qubit gates,[6–15] and extended coherence times.[2,3] However, the implementation of high-fidelity quantum gates still faces considerable challenges, among which noise arising from various mechanisms not only limits the coherence time of spin qubits but also hinders the scalability of quantum processors.[3,4] To address these issues, various quantum control techniques such as dynamical decoupling,[16] dynamically corrected gates,[17] pulse shaping,[5,18] and machine learning based feedback control[19–21] have been proposed and successfully implemented for both single- and two-qubit gates. In parallel, the exploration of alternative gate mechanisms provides promising opportunities to further enhance noise resilience and expand the range of available strategies for precise and scalable quantum control.

Geometric phase gates[22–26] have emerged as a promising approach for robust quantum control due to their inherent resilience to certain types of noise.[27,28] When a quantum system undergoes a cyclic evolution, it acquires a geometric phase determined solely by the global geometry of the trajectory in parameter space. In contrast to the dynamical phase, which depends on energy and evolution time. This geometric feature provides inherent robustness against specific noise.[27,28] Geometric phase gates are broadly classified into two categories:[25] adiabatic and nonadiabatic. Nonadiabatic geometric gates have attracted attention for enabling fast operations via cyclic trajectories driven in parameter space. Both theoretical and experimental studies have confirmed their robustness relative to dynamical gates.[27,28] Adiabatic geometric phase gates, on the other hand, rely on the ratio between control parameters rather than their absolute amplitudes,[26,29–34] which provides inherent robustness against amplitude fluctuations. In experimental implementations, adiabatic geometric phase gates have been realized by slowly varying the control fields to drive the qubit along closed loops in parameter space.[34–36] These approaches have demonstrated high-fidelity single- and two-qubit operations.[36]

However, most existing implementations rely on microwave control to drive qubits along specific trajectories,[25,28,34–36] making them susceptible to waveform distortions and control inaccuracies, similar to dynamical gates.

†Corresponding author. E-mail: cairanran@ustc.edu.cn
‡Corresponding author. E-mail: gcao@ustc.edu.cn

© 2025 Chinese Physical Society and IOP Publishing Ltd. All rights, including for text and data mining, AI training, and similar technologies, are reserved.

Moreover, microwave driving schemes can encounter challenges such as frequency crowding and crosstalk as the number of qubits increases. To address these issues, we propose a distinct implementation of adiabatic geometric phase gates based on rapid magnetic field modulation via square-wave current pulses. This approach exploits SOT to enable efficient and rapid switching of micromagnets.[37] Since the switching of each micromagnet can be completed within nanoseconds,[38] The entire gate operation is designed to complete within several tens of nanoseconds, which represents a practical balance between operation speed and the requirement of satisfying the adiabatic condition.[39] The use of square-wave control allows for relaxed waveform requirements and minimizes direct microwave exposure to the qubit. In addition, the discrete and stabilized nature of the magnetization states constrains the evolution trajectory to return to a well-defined final point, which helps suppress deviations caused by the noise. These characteristics contribute to the intrinsic robustness of the geometric phase and support a scalable and noise-resilient approach to fast geometric gate operations in spin-based quantum processors.

2. Adiabatic geometric single-qubit gate under magnetic field change

Consider an electron spin subjected to a time-dependent magnetic field, where the Hamiltonian is given by

$$H(t) = -\frac{\gamma}{2}\boldsymbol{B}(t)\cdot\boldsymbol{\sigma}, \tag{1}$$

Here, γ is the electron gyromagnetic ratio, $\boldsymbol{B}(t)$ is the time-dependent external magnetic field vector, and $\sigma = (\sigma_x, \sigma_y, \sigma_z)$ represents the Pauli matrices. At any time t, the system's eigenstates are expressed as

$$|\psi_+(t)\rangle = \cos\frac{\theta(t)}{2}|\uparrow\rangle + \mathrm{e}^{\mathrm{i}\phi(t)}\sin\frac{\theta(t)}{2}|\psi\rangle, \tag{2}$$

$$|\psi_-(t)\rangle = \sin\frac{\theta(t)}{2}|\uparrow\rangle - \mathrm{e}^{\mathrm{i}\phi(t)}\cos\frac{\theta(t)}{2}|\psi\rangle, \tag{3}$$

where $\theta(t)$ and $\phi(t)$ are the spherical coordinates describing the direction of the magnetic field.

When the external magnetic field $\boldsymbol{B}(t)$ evolves slowly (adiabatically) and forms a closed loop, the system undergoes adiabatic evolution. According to the adiabatic theorem, the electron spin remains in the instantaneous eigenstate of the Hamiltonian throughout the evolution. After completing the loop, the quantum state accumulates a dynamical phase γ_d and a geometric phase γ_g, resulting in the final state

$$|\psi(T)\rangle = \mathrm{e}^{\mathrm{i}\gamma_\mathrm{d}}\mathrm{e}^{\mathrm{i}\gamma_\mathrm{g}}|\psi(0)\rangle. \tag{4}$$

The dynamical phase is defined as

$$\gamma_\mathrm{d} = -\int_0^T \langle\psi(t)|H(t)|\psi(t)\rangle\,\mathrm{d}t. \tag{5}$$

The geometric phase, determined solely by the evolution path, is given by

$$\gamma_\mathrm{g} = \oint_C A_n(R)\cdot\mathrm{d}R, \tag{6}$$

where A_n is the Berry connection, and C represents the closed trajectory of the parameter $R(t)$.

After eliminating the dynamical phase with an appropriate method, the initially orthogonal quantum states evolve into the following expression:

$$|\psi_\pm(t)\rangle = \mathrm{e}^{\mp\mathrm{i}\gamma_\mathrm{g}}|\psi_\pm(0)\rangle, \tag{7}$$

which indicates that the entire evolution process corresponds to the unitary operator

$$U = \mathrm{e}^{-\mathrm{i}\gamma_\mathrm{g}\boldsymbol{n}_0\cdot\boldsymbol{\sigma}}, \tag{8}$$

where n_0 represents the initial quantum state's direction on the Bloch sphere. Physically, this evolution can be interpreted as a rotation around the n_0 axis by an angle of $-2\gamma_\mathrm{g}$. In other words, the evolution is equivalent to an SU(2) rotation on the Bloch sphere along the n_0 direction, with the rotation angle determined by the geometric phase γ_g. This property is of fundamental importance in geometric quantum computation, as it provides the theoretical foundation for constructing geometric quantum gates while also demonstrating the robustness of gate operations against certain types of errors due to the nature of geometric phases.

3. Realization of adiabatic geometric gates

In previous implementations, qubits were typically driven along closed trajectories in parameter space using microwave control, due to the difficulty of realizing fast and precise manipulation of magnetic fields. In this work, we adopt an alternative strategy by utilizing spin–orbit torque (SOT), which enables rapid and efficient magnetization switching by injecting an in-plane charge current into a heavy metal layer to generate a transverse spin current. This spin current exerts a torque on the adjacent ferromagnetic layer, allowing deterministic control of its magnetization direction and thus dynamic modulation of the magnetic field,[37] as illustrated in Fig. 1(c). This mechanism allows for the implementation of an adiabatic geometric phase gate through discrete field reorientation.

As illustrated in Figs. 1(a) and 1(b), the central region of the device contains a quantum dot with a single electron, forming a single-electron spin qubit. The quantum dot is surrounded by four switchable SOT-micromagnets, symmetrically arranged relative to the quantum dot, which are sequentially switched to generate a time-dependent closed magnetic field trajectory for geometric phase accumulation. A static external magnetic field is additionally applied to modulate the

shape of the magnetic trajectory, enabling precise and continuous control over the accumulated geometric phase. Each micromagnet is located at a lateral distance of 80 nm from the quantum dot, with dimensions of $(l, w, h) = (200, 100, 5)$ nm, where l, w, and h represent the length, width, and height of the micromagnet, respectively. Additionally, each micromagnet is positioned at a vertical height of 50 nm above the quantum dot.

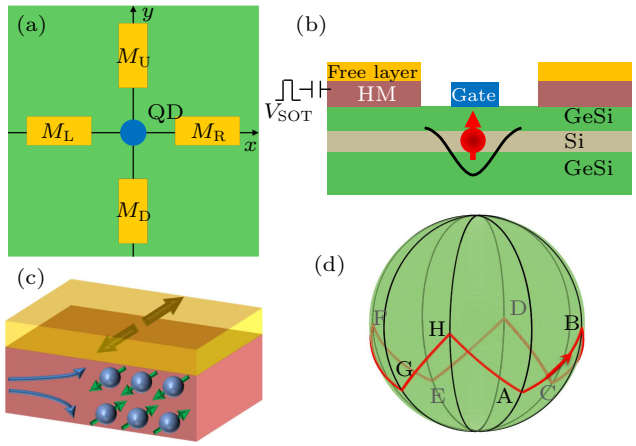


Fig. 1. Construction of closed magnetic field evolution paths using switchable micromagnets. (a) Schematic diagram of the device structure. The central region contains a single quantum dot occupied by one electron, forming a single-spin qubit located at the origin ($x = 0$, $y = 0$). Four switchable micromagnets are symmetrically arranged around the quantum dot. (b) Cross-sectional view along the x-axis from panel (a). Each switchable micromagnet consists of two layers: an upper magnetic material layer and a lower heavy metal layer. When a current flows through the heavy metal layer, the spin–orbit torque (SOT) induces magnetization switching in the magnetic material layer. (c) Schematic diagram of magnetization switching driven by SOT. When a charge current passes through a heavy metal material such as platinum (Pt), the strong spin–orbit coupling (SOC) in Pt causes spin-up and spin-down electrons to deflect in opposite directions. This results in a transverse spin current that is perpendicular to both the charge current direction and the spin polarization axis. The spin accumulation at the interface between the heavy metal and the micromagnets exerts a spin–orbit torque on the magnetization, which can drive the reversal of the magnetic orientation of the micromagnets. (d) Closed evolution path. The trajectory is formed by sequentially switching a single micromagnet at a time, creating a closed path. Under this path, the evolution of the qubit's eigenstate on the Bloch sphere is shown. The qubit starts at point A and follows a sequence through B to H before returning to A.

By adjusting the amplitude and duration of the applied current pulses, the switching speed of each micromagnet can be precisely controlled, enabling dynamic modulation of the magnetic field. To satisfy the adiabatic condition, the magnetization switching time is set to 10 ns. Furthermore, to ensure magnetic field stability during the gate operation, only one micromagnet is switched at a time. This sequential switching strategy avoids simultaneous switching and helps suppress non-ideal effects arising from field interference.

Since the four switchable micromagnets can assume 16 distinct magnetization states (as shown in Fig. S1 in the supplementary materials), we can flexibly select suitable configurations to construct different closed magnetic field trajectories, enabling path choices tailored to specific operational requirements. Based on the symmetry of the magnetic field distributions corresponding to different magnetization states, we simulate three distinct field distributions with different symmetries (as shown in Fig. S2 in the supplementary materials). Using these three magnetic field distributions, we further design a closed magnetic field trajectory to enable precise control of the geometric phase as shown in Fig. 1(d). Under different micromagnet configurations, the spin qubit experiences a total magnetic field B_{total}, which is the vector sum of the external magnetic field and the stray field generated by the micromagnet. The instantaneous eigenstate of the system Hamiltonian corresponding to each configuration can be represented as a point on the Bloch sphere, initially denoted as point A. By sequentially switching the micromagnet configurations, the eigenstate adiabatically evolves along a closed trajectory on the Bloch sphere, passing through points A $\rightarrow$ H, and eventually returning to point A.

When the external magnetic field is set to zero, the evolution path corresponding to trajectory originates from point A, progresses counterclockwise to H, and ultimately returns to A, forming a trajectory that is symmetric about the z-axis and the geometric phases accumulated along the trajectory is 1.32π. To further refine the evolution trajectory and achieve precise control over the accumulated geometric phase, the external magnetic field along the z-direction can be utilized to flexibly adjust both the shape of the closed path and the initial direction of the trajectory. By finely tuning the external magnetic field, the evolution of the qubit on the Bloch sphere can be modified, enabling precise control over the qubit's evolution.

As shown in Fig. 2(a), we investigate the influence of the external magnetic field on the geometric phase accumulated along the trajectory. In Fig. 2(a), the geometric phase corresponding to the trajectory is plotted as a function of the external magnetic field. We simulate the field increases from -0.1 T to 0.1 T. The geometric phase initially decreases gradually, then drops sharply, and eventually stabilizes. Notably, in the intermediate region of the field variation, the geometric phase exhibits the most pronounced sensitivity to magnetic field tuning.

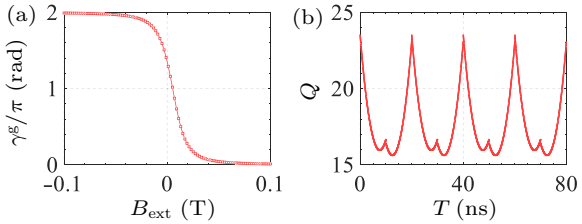


Fig. 2. Control of the evolution path via external magnetic field. (a) Regulation of path by the external magnetic field. By varying the strength of the external magnetic field along the z-direction, the directions of different points along the path and its geometric shape can be adjusted, leading to variations in the geometric phase accumulated over a full evolution cycle. (b) Time evolution of the quality factor Q for the loop. When the external field is set to -11.3 mT, the variation of Q over time is shown in the figure, demonstrating that Q remains above 12 throughout the evolution, thereby satisfying the adiabatic approximation.

This phenomenon arises from the interplay of two competing mechanisms. When the external magnetic field is strong, it dominates the trajectory evolution, leading to a smaller variation in the solid angle enclosed by the trajectory on the Bloch sphere. As a result, small adjustments to the external field induce only minor changes in the trajectory shape, resulting in limited variations in the geometric phase. In contrast, when the external magnetic field is weak, the local magnetic field generated by the controllable micromagnets becomes the dominant factor shaping the trajectory. In this regime, variations in the external magnetic field on the order of 10 mT can effectively modulate the geometric phase, allowing for extensive tunability of the geometric phase without exceeding the threshold required for stable and controllable micromagnet switching.[40,41]

To ensure that the system evolution satisfies the adiabatic approximation, we calculate the time dependence of the Q parameter,[36] defined as

$$Q = \frac{1}{\beta}, \tag{9}$$

where β represents the adiabatic parameter, given by

$$\beta = \left| \frac{\langle E_0(t)| \partial_t H(t) |E_1(t)\rangle}{(E_0(t) - E_1(t))^2} \right|. \tag{10}$$

Here, E_0 and E_1 denote the instantaneous eigenenergies of the system. According to the adiabatic approximation criterion, the system must satisfy $Q \gg 1$ to ensure adiabatic evolution, thereby minimizing non-adiabatic transitions and maintaining high-fidelity quantum control. In this study, we adopt $Q > 12$ as the threshold for adiabaticity, consistent with experimental benchmarks reported in the literature.[36]

As shown in Fig. 2(b), for an external magnetic field strength of -11.3 mT, the geometric phase per trajectory is $7\pi/4$, which is chosen because it corresponds to a $\pi/2$ rotation modulo 2π, a typical choice for demonstrating gate performance in experiments. we plot the time evolution of Q as a function of time. The results indicate that Q remains greater than 12 throughout the evolution, confirming the validity of the adiabatic approximation.

4. Influence of noise

To further evaluate the robustness of our scheme under realistic conditions, we consider two primary sources of magnetic field noise. In conventional microwave-driven geometric gate schemes, noise-induced fluctuations in the qubit frequency hinder precise control.[27] However, in our proposal, charge noise primarily leads to small spatial displacements of the qubit, resulting in effective modulation of the local magnetic field it experiences. The displacement induced by charge noise is only a few picometers,[3] and its effect on the qubit can therefore be neglected. The second noise source arises from the random flipping of magnetic domains during the switching process of micromagnets. We model this noise as a stationary, Gaussian, and Markovian process, whose statistical properties follow an Ornstein–Uhlenbeck (OU) process.[35] The noise has a Lorentzian power spectral density with a bandwidth Γ and a noise power P_i, where $i = \theta$, ϕ denotes the angular direction (elevation or azimuth) in which the noise is applied. Since the magnetic field produced by the micromagnets is well-defined once the switching is complete, the initial and final values of the noisy trajectory must remain fixed regardless of the fluctuations during the evolution. To satisfy this boundary condition, we modify the standard OU process into an Ornstein–Uhlenbeck bridge process,[42] which constrains the noise to vanish at both ends of the evolution.

To quantitatively analyze the impact of noise in different directions on the geometric phase gate, we independently simulated the effects of noise applied to the θ and ϕ directions. In our simulations, the noise amplitude is defined as $S_i = \sqrt{P_i}$. Figures 3(a) and 3(b) show the statistical distributions of the geometric phase for $S_\theta = 0.1$ and $S_\theta = 1$, respectively, with 10^4 samples generated in each case. As the comparison shows, the distribution broadens as the noise amplitude increases. By fitting the data with a Gaussian distribution, we obtain standard deviations of $\sigma = 0.0018$ and $\sigma = 0.0177$ for the two cases. Figures 3(d) and 3(e) present the geometric phase distributions for $S_\phi = 0.1$ and $S_\phi = 1$, respectively, with corresponding standard deviations of $\sigma = 0.0018$ and $\sigma = 0.0183$. These results are similar to those obtained for noise in the θ direction.

Based on the expression[35]

$$\nu = \mathrm{e}^{-(4\sigma)^2/2}, \tag{11}$$

we evaluate how the noise amplitude affects the coherence of the geometric phase gate. Figure 3(c) shows the dependence of the coherence ν on the noise amplitude S_θ. As expected, the coherence decreases with increasing noise amplitude. In contrast to conventional microwave-driven schemes,[35] which show significant coherence degradation at noise amplitudes $S = 1$, our protocol preserves high coherence even under similarly strong noise conditions. This is because in microwave driving schemes, the noise is typically modeled as a standard OU process, which means the presence of noise causes the system's evolution path to deviate significantly from the ideal trajectory, leading to non-closed loops and thus decreasing the geometric phase fidelity. In contrast, our scheme employs a magnetic field rotation implemented via micromagnet switching. Although noise may perturb the field trajectory during the switching process, the field eventually returns to a well-defined final value. This feature effectively introduces a set of anchor points along the evolution path, thereby suppressing noise-induced deviations throughout the trajectory. As a result, the system's evolution remains closed even under strong noise conditions, significantly enhancing the robustness of the geometric phase gate.

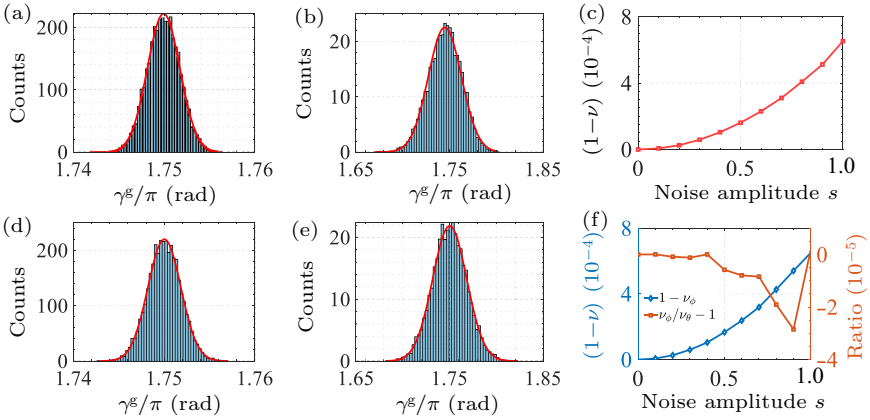


Fig. 3. Effects of magnetic noise on the geometric phase. In all simulations, the external magnetic field is set to -11.3 mT, corresponding to an ideal (noise-free) geometric phase of 1.75π accumulated over the closed trajectory. (a) Statistical distribution of the geometric phase under elevation-angle noise with amplitude $S_\theta = 0.1$. Gaussian fit yields $\mu = 1.7499$, $\sigma = 0.0018$. (b) The same as panel (a), but with increased noise amplitude $S_\theta = 1$. Gaussian fit yields $\mu = 1.7450$, $\sigma = 0.0177$. (c) Evolution of the coherence loss, quantified by $1-\nu$, as a function of elevation-angle noise amplitude S_θ. (d) Statistical distribution of the geometric phase under azimuthal-angle noise with amplitude $S_\phi = 0.1$. Gaussian fit yields $\mu = 1.7500$, $\sigma = 0.0018$. (e) The same as panel (d), but with increased noise amplitude $S_\phi = 1$. Gaussian fit yields $\mu = 1.7502$, $\sigma = 0.0183$. (f) Left axis (blue): $1-\nu_\phi$, indicating the coherence loss under azimuthal noise. Right axis (orange): $\nu_\theta/\nu_\phi - 1$, showing the relative difference in coherence between elevation and azimuthal noise.

Figure 3(f) further compares the effects of noise applied to the θ and ϕ directions. It shows that the difference in coherence decrease between the two noise types is relatively small. This is because the evolution path of the qubit on the Bloch sphere does not follow a purely meridional or latitudinal trajectory. As a result, both types of angular noise contribute to the overall error of the geometric gate.

5. Influence of positional deviation

In practical experiments, charge noise can cause deviations of the electron position from its ideal location by perturbing the electron wavefunction. Additional contributing factors include structural imperfections introduced during sample fabrication and potential modulation by electrode voltages. The combined effects of these factors can lead to deviations in the system's evolution from the intended trajectory, resulting in inaccuracies in the accumulated geometric phase and a shift in the rotation axis n_0. Consequently, these deviations degrade the fidelity of the quantum operation.

To quantitatively assess the impact of positional deviation on the system, figure 4(a) illustrates the variation in the accumulated geometric phase as the qubit position shifts within the xy-plane. At the ideal position, the geometric phase accumulated over one closed-loop evolution is $\gamma^g_{\text{ideal}} = 7\pi/4$. Each point in the figure represents the difference in the accumulated geometric phase due to a positional offset $(\delta x, \delta y)$, defined as $\Delta\gamma^g = \gamma^g_{\text{ideal}} - \gamma^g$. As shown in the figure, the geometric phase deviation exhibits central symmetry about the origin. Even when the positional offset reaches 10 nm, the deviation in the accumulated geometric phase remains below 1%.

Figure 4(b) illustrates the variation in quantum gate fidelity as a function of positional deviation. The infidelity is computed using the formula

$$I = 1 - \frac{\left|\text{tr}\left[UU_0^{-1}\right]\right|}{2}, \tag{12}$$

where U_0 and U represent the evolution operators in the absence and presence of positional deviation, respectively. In this calculation, the dynamical phase has been eliminated using the echo method.

Unlike Fig. 4(a), the fidelity does not exhibit central symmetry about the origin. This asymmetry arises because positional deviations not only introduce errors in the geometric phase but also alter the rotation axis n_0. Nevertheless, even when the positional deviation reaches 10 nm, the infidelity remains below 10^{-3}, indicating that the proposed scheme exhibits strong robustness against positional variations.

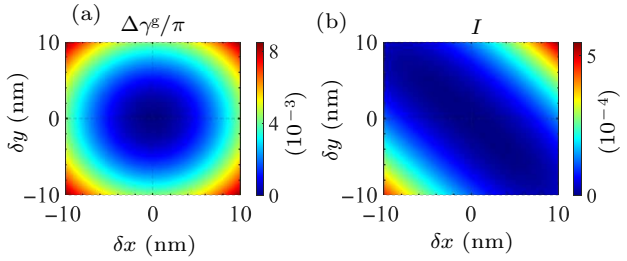


Fig. 4. Influence of positional deviation on geometric behavior and gate infidelity. (a) Effect of xy-directional positional deviation on the geometric phase. The simulation under a constant external magnetic field of -11.3 mT. In the absence of positional deviation, the accumulated geometric phase is 1.75π. Each point in the figure represents the difference between the accumulated geometric phase under positional deviation and the geometric phase in the ideal case, where the trajectory of the loop is altered due to the positional shift. (b) Effect of xy-directional positional deviation on the fidelity of the geometric gate. Based on the results in panel (a), we further account for the impact of positional deviation on the rotation axis n_0 and compute the corresponding geometric phase gate infidelity.

6. Discussion and conclusion

Our proposed scheme exhibits strong robustness against positional deviations and external field variations, making it a promising approach for implementing geometric phase gates in quantum computing. However, several key challenges require further investigation. One critical concern in practical applications is the heating effect during the magnetization switching process. This issue can be mitigated through var-

ious strategies. For instance, utilizing heavy metals with a larger spin Hall angle can significantly reduce the power required for switching.[38] Additionally, the thermal load on the system can be reduced through thermal isolation techniques, such as deep silicon etching, as well as by employing high-temperature qubits.[8,43,44] Another challenge lies in the trade-off between robustness and gate speed. A fundamental limitation of adiabatic geometric phase gates is the requirement to satisfy the adiabatic approximation,[34,36] which often leads to long operation times. To address this issue, we can optimize the structure and shape of the micromagnets,[45] enabling the construction of smoother closed trajectories. This enhancement improves the Q value during the evolution process, allowing the geometric phase gate to operate within a shorter time while maintaining robustness.

In summary, we proposed a robust scheme for implementing geometric phase gates in silicon quantum computing, utilizing a precisely controlled magnetic field trajectory. By employing four switchable micromagnets, we constructed closed evolution paths that enable precise control over the accumulated geometric phase. Our results reveal strong resilience of the proposed approach to magnetic field fluctuations and spatial deviations, underscoring its suitability for scalable implementation of geometric phase gates. This study provides a promising pathway toward the scalable realization of geometric phase gates, with potential applications in fault-tolerant quantum computing. Future work will focus on experimental validation and further optimization of system robustness under realistic noise conditions.

Acknowledgements

Project supported by the National Natural Science Foundation of China (Grant Nos. 12304560, 92265113, 12074368, and 12034018), the Innovation Program for Quantum Science and Technology (Grant No. 2021ZD0302300), and China Postdoctoral Science Foundation (Grant Nos. BX20220281 and 2023M733408).

References

[1] Loss D and DiVincenzo D P 1998 *Phys. Rev. A* **57** 120
[2] Veldhorst M, Hwang J, Yang C, Leenstra A, de Ronde B, Dehollain J, Muhonen J, Hudson F, Itoh K M and Morello A T 2014 *Nat. Nanotechnol.* **9** 981
[3] Yoneda J, Takeda K, Otsuka T, Nakajima T, Delbecq M R, Allison G, Honda T, Kodera T, Oda S and Hoshi Y 2018 *Nat. Nanotechnol.* **13** 102
[4] Vinet M 2021 *Nat. Nanotechnol.* **16** 1296
[5] Yang C, Chan K, Harper R, Huang W, Evans T, Hwang J, Hensen B, Laucht A, Tanttu T and Hudson F 2019 *Nat. Electron.* **2** 151
[6] O'Brien J L, Pryde G J, Gilchrist A, James D F, Langford N K, Ralph T C and White A G 2004 *Phys. Rev. Lett.* **93** 080502
[7] He Y, Gorman S, Keith D, Kranz L, Keizer J and Simmons M 2019 *Nature* **571** 371
[8] Petit L, Eenink H, Russ M, Lawrie W, Hendrickx N, Philips S, Clarke J, Vandersypen L and Veldhorst M 2020 *Nature* **580** 355
[9] Mądzik M T, Asaad S, Youssry A, Joecker B, Rudinger K M, Nielsen E, Young K C, Proctor T J, Baczewski A D and Laucht A 2022 *Nature* **601** 348
[10] Mills A R, Guinn C R, Gullans M J, Sigillito A J, Feldman M M, Nielsen E and Petta J R 2022 *Sci. Adv.* **8** eabn5130
[11] Noiri A, Takeda K, Nakajima T, Kobayashi T, Sammak A, Scappucci G and Tarucha S 2022 *Nature* **601** 338
[12] Xue X, Russ M, Samkharadze N, Undseth B, Sammak A, Scappucci G and Vandersypen L M 2022 *Nature* **601** 343
[13] Dijkema J, Xue X, Harvey-Collard P, Rimbach-Russ M, de Snoo S L, Zheng G, Sammak A, Scappucci G and Vandersypen L M K 2025 *Nat. Phys.* **21** 168
[14] McMillan S R and Burkard G 2023 *Phys. Rev. B* **108** 125414)
[15] Tanttu T, Lim W H, Huang J Y, Stuyck N D, Gilbert W, Su R Y, Feng M, Cifuentes J D, Seedhouse A E, Seritan S K., Ostrove C I, Rudinger K M, Leon R C C, Huang W, Escott C C, Itoh K M, Abrosimov N V, Pohl H J, Thewalt M L W, Hudson F E, Blume-Kohout R, Bartlett S D, Morello A, Laucht A, Yang C H, Saraiva A and Dzurak A S 2024 *Nat. Phys.* **20** 1804
[16] Hahn E L 1950 *Phys. Rev.* **80** 580
[17] Wang X, Bishop L S, Kestner J, Barnes E, Sun K and Das Sarma S 2012 *Nat. Commun.* **3** 997
[18] Emerson J 2019 *Nat. Electron.* **2** 140
[19] Daraeizadeh S, Premaratne S P and Matsuura A Y 2020 *IEEE International Conference on Quantum Computing and Engineering (QCE)* pp. 30–36
[20] Lapointe-Major M, Germain O, Camirand Lemyre J, Lachance-Quirion D, Rochette S, Camirand Lemyre F and Pioro-Ladrière M 2020 *Phys. Rev. B* **102** 085301
[21] Nakajima T, Kojima Y, Uehara Y, Noiri A, Takeda K, Kobayashi T and Tarucha S 2021 *Phys. Rev. Appl.* **15** L031003
[22] Johansson M, Sjöqvist E, Andersson L M, Ericsson M, Hessmo B, Singh K and Tong D 2012 *Phys. Rev. A* **86** 062322
[23] Sjöqvist E, Tong D M, Andersson L M, Hessmo B, Johansson M and Singh K 2012 *New J. Phys.* **14** 103035
[24] Solinas P, Zanardi P, Zanghí N and Rossi F 2003 *Phys. Rev. B* **67** 121307
[25] Zhang J, Kyaw T H, Filipp S, Kwek L C, Sjöqvist E and Tong D 2023 *Phys. Rep.* **1027** 1
[26] Zanardi P and Rasetti M 1999 *Phys. Lett. A* **264** 94
[27] Zhang C, Chen T, Li S, Wang X and Xue Z Y 2020 *Phys. Rev. A* **101** 052302
[28] Ma R L, Li A R, Wang C, Kong Z Z, Liao W Z, Ni M, Zhu S K, Chu N, Zhang C and Liu D 2024 *Phys. Rev. Appl.* **21** 014044
[29] Pachos J, Zanardi P and Rasetti M 1999 *Phys. Rev. A* **61** 010305
[30] Falci G, Fazio R, Palma G M, Siewert J and Vedral V 2000 *Nature* **407** 355
[31] Duan L M, Cirac J I and Zoller P 2001 *Science* **292** 1695
[32] Solinas P, Zanardi P, Zanghì N and Rossi F 2003 *Phys. Rev. A* **67** 062315
[33] Toyoda K, Uchida K, Noguchi A, Haze S and Urabe S 2013 *Phys. Rev. A* **87** 052307
[34] Wu H, Gauger E M, George R E, Möttönen M, Riemann H, Abrosimov N V, Becker P, Pohl H J, Itoh K M and Thewalt M L 2013 *Phys. Rev. A* **87** 032326
[35] Berger S, Pechal M, Abdumalikov Jr A A, Eichler C, Steffen L, Fedorov A, Wallraff A and Filipp S 2013 *Phys. Rev. A* **87** 060303
[36] Huang Y Y, Wu Y K, Wang F, Hou P Y, Wang W B, Zhang W G, Lian W Q, Liu Y Q, Wang H Y and Zhang H Y 2019 *Phys. Rev. Lett.* **122** 010503
[37] Cai R, Li F G, Wang B C, Li H O, Cao G and Guo G P 2025 *Phys. Rev. Appl.* **23** 024048
[38] Shao Q, Li P, Liu L, Yang H, Fukami S, Razavi A, Wu H, Wang K, Freimuth F and Mokrousov Y 2021 *IEEE Trans. Magn.* **57** 1
[39] Holstein B R 1989 *Am. J. Phys* **57** 1079
[40] Fukami S, Anekawa T, Zhang C and Ohno H 2016 *Nat. Nanotechnol.* **11** 621
[41] Kong W, Wan C, Tao B, Fang C, Huang L, Guo C, Irfan M and Han X 2018 *Appl. Phys. Lett.* **113** 162402
[42] Mazzolo A 2017 *Journal of Mathematical Physics* **58** 093302
[43] Yang C H, Leon R, Hwang J, Saraiva A, Tanttu T, Huang W, Camirand Lemyre J, Chan K W, Tan K and Hudson F E 2020 *Nature* **580** 350
[44] Camenzind L C, Geyer S, Fuhrer A, Warburton R J, Zumbühl D M and Kuhlmann A V 2022 *Nat. Electron.* **5** 178
[45] Yang J C, Li Z H, Wang B C, Li H O, Cao G and Guo G P 2023 *Appl. Phys. Lett.* **122** 054001